

Infusion Mechanisms in Brain White Matter and Their Dependence on Microstructure: An Experimental Study of Hydraulic Permeability

Asad Jamal¹, Maria Teresa Mongelli, Marco Vidotto, Michael Madekurozwa, Andrea Bernardini, Darryl R. Overby², Elena De Momi³, Ferdinando Rodriguez y Baena⁴, Joseph M. Sherwood⁵, and Daniele Dini⁶

Abstract—Objective: Hydraulic permeability is a topic of deep interest in biological materials because of its important role in a range of drug delivery-based therapies. The strong dependence of permeability on the geometry and topology of pore structure and the lack of detailed knowledge of these parameters in the case of brain tissue makes the study more challenging. Although theoretical models have been developed for hydraulic permeability, there is limited consensus on the validity of existing experimental evidence to complement these models. In the present study, we measure the permeability of white matter (WM) of fresh ovine brain tissue considering the localised heterogeneities in the medium using an infusion-based experimental set up, *iPerfusion*. We measure the flow across different parts of the WM in response to applied pressures for a sample of specific dimensions and calculate the permeability from directly measured parameters. Furthermore, we directly probe the effect of anisotropy of the tissue on permeability by considering the directionality of tissue on the obtained values. Additionally, we investigate whether WM hydraulic permeability changes with post-mortem time. To our knowledge, this is the first report of experimental measurements of the localised WM permeability, also demonstrating the effect of axon directionality on

permeability. This work provides a significant contribution to the successful development of intra-tumoural infusion-based technologies, such as convection-enhanced delivery (CED), which are based on the delivery of drugs directly by injection under positive pressure into the brain.

Index Terms—Convection-enhanced delivery, directionality of axons, hydraulic permeability, infusion-based flow, ovine brain tissue.

I. INTRODUCTION

GLIOBLASTOMA multiforme (GBM), a grade IV glioma, is the most aggressive and frequently diagnosed form of primary central nervous system (CNS) tumour in adults, with an average age of 64. Studies have reported an incidence of 5 per 100,000 persons and GBM leads to 250,000 deaths per year worldwide [1], [2]. Conventional techniques for GBM treatment, such as radiation and chemotherapy, have either severe side effects (*e.g.* localised tissue damage) or suffer from limitations in passing through the blood-brain barrier (BBB) and distribution of therapeutic agents throughout the tissue by passive diffusion [3]–[5]. To overcome these challenges, applications of robotically steered needles in neurosurgery is gaining momentum [6], with important new solutions and strategies been developed and studied; further details on this topic can be found in the recent review article by Audette *et al.* [7]. Convection-enhanced drug delivery [8], [9], an intra-tumoural infusion method for localised drug delivery, has emerged as a viable delivery technique and a promising solution to overcome some of the mentioned obstacles. In contrast to diffusion-based drug delivery techniques, which rely on concentration gradients to drive the flow, CED is based on infusion under a positive pressure gradient into the CNS. By utilising advective transport, CED enables relatively lower concentrations of the therapeutic agent than diffusion-based delivery methods. CED is not without limitations and its efficiency is affected by a number of factors, including target heterogeneity, WM edema and transport parameters. Furthermore, lack of histological information of brain tissue leads to issues in determining the ratio of the drug distribution volume to the infusion volume, $R_{d/i}$ ($V_d:V_i$), where V_d is drug distribution volume and V_i is drug infusion volume [9], [10], which is conventionally used to assess the efficacy of CED.

Manuscript received April 28, 2020; revised August 3, 2020; accepted September 3, 2020. Date of publication September 15, 2020; date of current version March 19, 2021. This work was supported by EDEN2020, a project funded by the European Union's H2020 Research and Innovation Programme under Grant agreement No. 688279. DD also acknowledges support received from the Engineering and Physical Sciences Research Council (EPSRC) through his Established Career Fellowship EP/N025954/1. JMS acknowledges support received from the Royal Academy of Engineering Research Fellowship RF2016\16\18. A. Jamal and M.T. Mongelli contributed equally to this manuscript. (Corresponding author: Asad Jamal.)

Asad Jamal is with the Department of Mechanical Engineering, Imperial College London, London SW7 2AZ, U.K. (e-mail: a.jamal@imperial.ac.uk).

Maria Teresa Mongelli is with the Department of Mechanical Engineering, Imperial College London, and also with the Department of Electronics, Information and Bioengineering, Politecnico di Milano.

Marco Vidotto and Elena De Momi are with the Department of Electronics, Information and Bioengineering, Politecnico di Milano.

Michael Madekurozwa, Darryl R. Overby, and Joseph M. Sherwood are with the Department of Bioengineering, Imperial College London.

Andrea Bernardini, Ferdinando Rodriguez y Baena, and Daniele Dini are with the Department of Mechanical Engineering, Imperial College London.

This article has supplementary downloadable material available at <https://ieeexplore.ieee.org>, provided by the authors.

Digital Object Identifier 10.1109/TBME.2020.3024117

For a given pressure gradient, flow through a porous tissue can be characterised by Darcy's law and the *hydraulic permeability*, κ , which represents a geometry and viscosity corrected conductance (reciprocal of resistance to flow). However, in heterogeneous and anisotropic tissues, resistance to fluid flow is both location and direction dependent and consequently it dictates the ratio $R_{d/i}$ [11]. Therefore, determining the hydraulic permeability of multiphase tissues is key for the development and successful implementation of intra-tumour infusion-based drug delivery therapies that rely on advective transport mechanisms [12]–[14]. It also plays a fundamental role in determining transport of interstitial molecules [15], [16], which is strongly linked to many physiological processes of the brain, including dynamics of pathological molecules that transit the extracellular matrix (ECM) [17]–[19].

In contrast to rigid porous materials, wherein κ is constant, hydraulic permeability in biological materials has been reported to vary with tissue deformation that occurs due to the pressure gradient during intra-tumoural infusion [20]. Hydraulic permeability also has a large dependence on pore structure topology and tissue geometry [21]. For brain tissue, there is limited knowledge of these parameters, and a lack of reliable methodologies for their accurate determination, which makes it difficult to understand infusion mechanisms and determine the hydraulic permeability in a predictive manner.

For cerebral tissue, although theoretical models have been developed to determine hydraulic permeability, less attention has been paid to experimental studies. Furthermore, the constitutive parameters used in theoretical models vary by up to three orders of magnitude [22]–[27]. Such a significant difference across the literature and lack of experimental evidence to complement these models makes it difficult to justify the use of specific values for predictive purposes, *e.g.* when they need to be used as inputs for large scale CED simulations. Furthermore, mechanical behaviour such as stiffness of anisotropic biological tissues which are composed of directional fibres *e.g.* meniscal tissue [28] is known to be affected by the directionality of fibres [29]. Therefore, a deeper understanding of the effect of tissue microstructural features is needed to predict the local response of the system to external infusion and physiological processes; what is the effect of fibre bundle orientation on hydraulic permeability? This ought to be characterised and reproduced with the most accurate available methods.

There are a number of available techniques for estimating hydraulic permeability experimentally. These techniques include infusion, *i.e.* localised drug delivery to a tissue from a point source (catheter's tip) [30]–[32], perfusion, *i.e.* drug delivery from a source with cross sectional surface comparable to the tissue dimensions [31], [33], [34] and compression [35], [36]. Due to heterogeneity of local tissue microstructure, differences in where the sample comes from and sample size between these techniques makes it difficult to compare results and may have led to the large range of reported values.

In the case of brain tissue, only a few studies have experimentally determined hydraulic permeability, but their results are affected by the sample and experimental protocol adopted. Franceschini *et al.* [37] performed an *ex vivo* uniaxial deformation experiment on human brain tissue excised within

12h of death and indirectly determined permeability from the compressibility parameters by fitting the data to Terzaghi's theory. Tavner *et al.* [23], used a perfusion experiment to determine the hydraulic conductivity (which can be directly linked to permeability) of lamb and sheep brains using Darcy's law. However, both studies adopted large samples (30 mm/5-8 mm initial diameter/height) to study the macroscopic tissue response and did not consider the microscale localised heterogeneities in the tissue. Brain is composed of cerebrospinal fluid, grey matter and WM, and is anisotropic due to the directionality of axons in WM. Also, the perfusion based experimental set up used by Tavner *et al.* [23] is not compatible with the CED, which instead requires an infusion-based approach. Furthermore, the effect of post-mortem time on hydraulic permeability has not been investigated previously. In order to improve understanding of drug transport within brain matter, more information about differences between grey matter and WM, and anisotropy in the tissue are required.

WM anisotropy, due to directionality of axons in the matrix [38], [39], makes WM hydraulic permeability direction-dependent. This detail is often overlooked, and only a few theoretical studies have reported the effect of anisotropy of brain WM on the hydraulic permeability [40]. To the best of our knowledge no experimental study has considered the anisotropy of WM at the millimetre and sub-millimetre scales or has investigated the effect of directionality of axons on hydraulic permeability.

The present study is aimed at experimentally determining brain tissue localised hydraulic permeability and to quantify its dependence on tissue microstructure, with focus on axon orientation. We perform experiments on fresh ovine brain and, in contrast to previously reported work, we determine the localised hydraulic permeability of WM from directly measured parameters using an infusion-based experimental set up, *iPerfusion* [41]. We measure the flow across a specific part of WM in response to applied pressures and calculate the permeability for a sample of specific dimensions. Furthermore, we explore if the hydraulic permeability of WM changes with post-mortem time. We also investigate the effect of anisotropy of WM on the hydraulic permeability and, to the best of our knowledge, we provide the first experimental investigation reporting the effect of directionality of axons on the hydraulic permeability of WM.

II. MATERIALS AND METHODS

A. Sample Preparation

Fresh ovine brains were arranged from a local slaughterhouse, and separate slices of 7-8 mm in thickness were made by cutting along coronal and sagittal directions. These cuts expose the cerebral WM from two perpendicular directions as shown in Fig. 1(a,b). The matrix of cerebral WM is mainly composed of two constituents, the axons and extracellular matrix. In coronal cut slices, the axons are parallel to the surface whereas in sagittal cuts they are perpendicular to the surface, as represented by black dots and lines in the schematic representation shown in Fig. 1(a). Using sharp blades, elongated specimens were obtained from a specific part of WM, corona radiata, and were carefully inserted in transparent plastic tubes of 5 mm inner diameter and 7 mm length. Special attention was paid to the size of the sample while

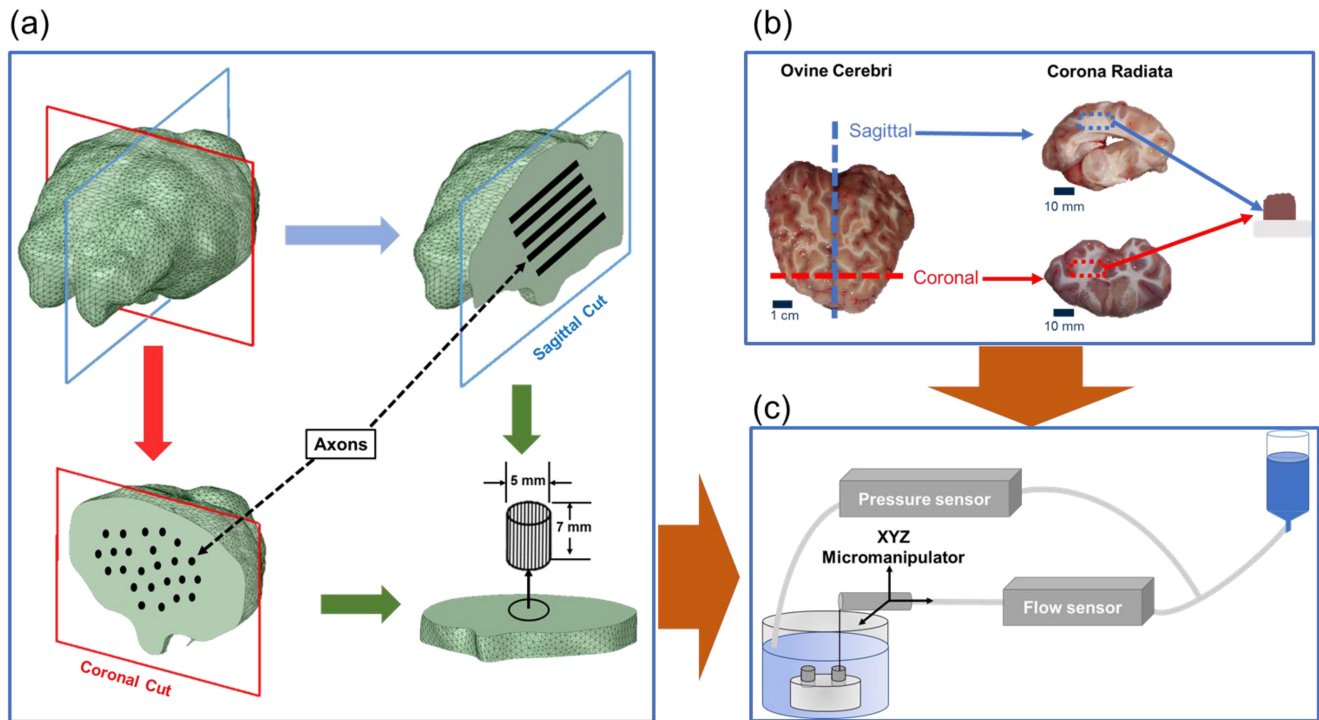


Fig. 1. (a) Schematic representation of slicing the ovine brain along coronal and sagittal cuts showing the directionality of axons in WM and making of a tube shaped sample from the slice, (b) representative picture of ovine brain and the coronal and sagittal cut slices, where the corona radiata part of WM used for making the sample is highlighted by dashed rectangles and (c) schematic representation of the experimental set up including the plastic petri dish showing samples suspended in a glass bath filled with PBS.

cutting, in order to avoid excessive deformation during insertion into the tube. In the samples from coronal cut slices, the axons were parallel to the long axis of the tube (S_{\parallel}), whereas in samples from sagittal cut slices (S_{\perp}), the axons were perpendicular to the long axis of the tube.

During the slicing of the brain, phosphate-buffered saline (PBS) was sprayed on the tissue in order to keep it hydrated. A plastic petri dish with custom made holes was used to hold the samples suspended in a glass bath filled with PBS at room temperature as shown in Fig. 1(c) to avoid dehydration of the tissue during the experiments.

To calculate hydraulic permeability from directly measured parameters, we used *iPerfusion* (Fig. 1(c)), developed to determine flow-pressure relationship in soft tissues as described elsewhere [41]. The system uses an actuated reservoir to control the pressure drop across the tissue, while recording the flow rate through the tissue with a thermal flow sensor (Sensirion SLG150), with an accuracy of approximately 5 nl/min.

The pressure is measured with a differential pressure transducer (Omegadyne PX409), with an accuracy of 0.04 mmHg. A needle (BD MicrolanceTM; stainless steel; 30G \times 1/2"; 0.3 \times 13mm) was connected to a micromanipulator for insertion into the WM sample.

B. Experimental Protocol and Data Acquisition

Prior to each acquisition, the pressure and flow sensors were calibrated. The needle was then inserted in the sample so that

tip was in the middle of the sample, *i.e.* for a 7 mm long sample needle was inserted 3.5 mm. The sample was completely immersed in PBS, which was also the infusate, at room temperature. An initial pressure of 7 mmHg was applied and was held until a stable condition for the flow rate was reached. This acclimatisation took 25-30 minutes and allowed the brain sample to adapt to the experimental environment.

An automated protocol of discrete applied pressure steps was then carried out, consisting of 10, 12.5, 15, 17.5, 20, 22.5 and 25 mmHg. For each step, the slope of the flow rate was estimated by linear regression over a moving window of 300s and continuously monitored. Steady state was defined as when the slope was continuously less than 5 nl/min/min for 60s, and the subsequent step was then applied. The last 4 minutes of stable data step was extracted, a Savitzky-Golay filter with a 60 second half-width was applied to reduce noise, and the average values of the filtered signals were used to represent that steady pressure and flow values.

To determine tissue hydraulic permeability from the experimental data, flow-pressure analysis on the flow rate and pressure traces was performed using the model [41]

$$Q = \kappa P \left(\frac{A}{L\mu} \right) = \kappa_r \left(\frac{P}{P_r} \right)^{\beta} \left(\frac{A}{L\mu} \right) \quad (1)$$

where Q is flow rate, P is the applied pressure drop across the tissue, A and L are the cross-sectional area and length of sample respectively and μ is the viscosity of the infused fluid. The pressure-dependence of hydraulic permeability is modelled

using $\kappa = \kappa_r \left(\frac{P}{P_r}\right)^\beta$, where κ_r is the hydraulic permeability at reference pressure P_r and the exponent β characterises the dependence of κ on pressure. In this study, we chose $P_r = 10$ mmHg as representative of physiological CSF pressure in adults [42].

It should be noted that the full tissue length was used here to evaluate permeability; the assumption made here, whose validity has been checked and confirmed via poro-elastic simulations of the infusion process performed using the finite element method similar to those performed in [40] but for the samples under investigation here, is that the infused fluid exudes from both end of the tubes containing the samples.

Fig. 2 shows representative flow rate and pressure traces with respect to time (a,b), and steady state flow rate (c) and hydraulic permeability for each applied pressure (d) for sample S_{\parallel} (blue) and S_{\perp} (red) cases. Figs 2(e,f) schematically represent the flow orientation with respect to the axon bundles.

Experiments were repeated on samples of corona radiata from different lamb brains. In total 71 brain samples with post-mortem time ranging from 3 to 24h were used to collect the experimental data.

It was not always possible to count each step as in some samples higher pressure steps did not achieve the steady state condition and were therefore excluded from data analysis. Only those samples were included for which at least three consecutive pressure steps (as shown in Fig. 2(a)) achieved the steady state condition and no anomalies were found in the instantaneous response to consecutive pressure rises. After quality control, 50 samples were analysed for the results presented in this work. Analysis of all flow rate and pressure traces along with raw data are provided in the Supporting Information.

III. RESULTS AND DISCUSSION

A. Effect of Directionality of Axons on Hydraulic Permeability

For statistical analysis, the average κ_r of each sample was used (*i.e.* the average of all pressure steps for that sample). Shapiro-Wilk tests on κ_r rejected normality for both S_{\parallel} and S_{\perp} samples ($p < 10^{-3}$), but did not reject lognormality ($p = 0.48$ and 0.17 respectively), hence analysis was carried out on the log of κ_r . An overview of the hydraulic permeability data for S_{\parallel} and S_{\perp} samples is shown in Fig. 3.

For S_{\parallel} samples, the average hydraulic permeability was $\kappa_r = 2.0 [1.3, 3.0] \times 10^{-16}$ m² (geometric mean, [95% confidence interval]), while S_{\perp} samples yielded $\kappa_r = 0.7 [0.6, 1.0] \times 10^{-16}$ m². The hydraulic permeability was thus 65 [44,78]% lower in S_{\perp} than S_{\parallel} samples (independent 2-tailed *t*-test, $p = 0.0002$). This trend is in line with what can be predicted by modelling the flow behaviour due to anisotropy through a composite material consisting of impermeable coarse fibres embedded in a fine matrix as proposed *e.g.* by Ethier [43]. However, considering that, as reported by Sykova et al. [44], the volume fraction of fibres in the tissue is ~ 70 -80%, a direct quantitative comparison with Ethier's model, which is most accurate for small fibres volume fraction (up to 30%), would prove inaccurate.

These results confirm that the flow across the tissue is strongly dependent on the local mechanical microenvironment. The WM matrix is composed of aligned myelinated axons and relatively soft extracellular matrix [45]. In the case of S_{\parallel} , the cross sectional area of the tissue exposed to infusate pressure is composed of both axons and the relatively soft ECM, whereas in the case of S_{\perp} , the exposed cross-sectional area is predominantly composed of axons [39]. It is harder to deform axons (stiffness of a single axon reported to be *e.g.* $E = 9.5$ kPa [46]) than ECM (E in the order of a few hundred pascals [47]). Therefore, during infusion, depending on the directionality in the tissue, the infusate faces different mechanical environments. Previously it has been reported that in WM, interstitial flow is more rapid in perivascular space and along the axons [48], [49]. Also, interstitial flow is impacted by convection driven flow. In CED, catheter delivers a volume of infusate to the targeted part of the tissue; this also increases interstitial flow in the surrounding parenchyma because of the pressure differential [50]. This suggests that if diffusion driven interstitial flow is more rapid in perivascular space and along the axons, then convection driven flow will have similar behaviour. Our results also advocate this environment dependency of flow in the tissue. In the case of S_{\parallel} , when the axons are aligned to the injection direction, the hydraulic permeability is higher, whereas in case of S_{\perp} , the axons are perpendicular to the fluid, and the hydraulic permeability is lower. These results clearly demonstrate that infusion across the WM tissue is strongly influenced by its intrinsic anisotropy. Therefore, the directionality of axons in the tissue should be considered when interpreting underlying infusion mechanisms within WM.

Our hydraulic permeability values of the ovine brain WM are the first experimentally determined values that consider localisation and tissue anisotropy. Franceschini *et al.* [37] and Tavner *et al.* [23] experimentally studied the permeability of brain tissue without considering the directionality in the tissue. Furthermore, their reported value of permeability is obtained using large samples of WM; hence, they can only represent homogenised isotropic macroscopic values of permeability. These issues make it inappropriate to compare our results with other experimental results in the literature. It is, however, worth noting that the values obtained in our experiments seem to confirm the disparity in permeability predicted when considering microstructural effects and different orientations of infusion, as reported in previous theoretical and numerical studies, *e.g.* see effect of tissue anisotropy on drug flow in [40] or the computed value of hydraulic permeability of corpus callosum (1.33×10^{-16} m²) reported in [22].

While in this paper we focus on direct deterministic measurements of hydraulic permeability using an infusion-based apparatus, it is worth mentioning the potential use of alternative inverse methodologies, such as Bayesian inference or other stochastic models, for the determination of specific material parameters of interest. Such methodologies, which have been successfully used for the determination of *e.g.* materials linear and non-linear characteristics, viscoelasticity, anisotropy and multi-scale parameters in fibre composites [51]–[54], can also shed light on the choice of model and model uncertainty [55]

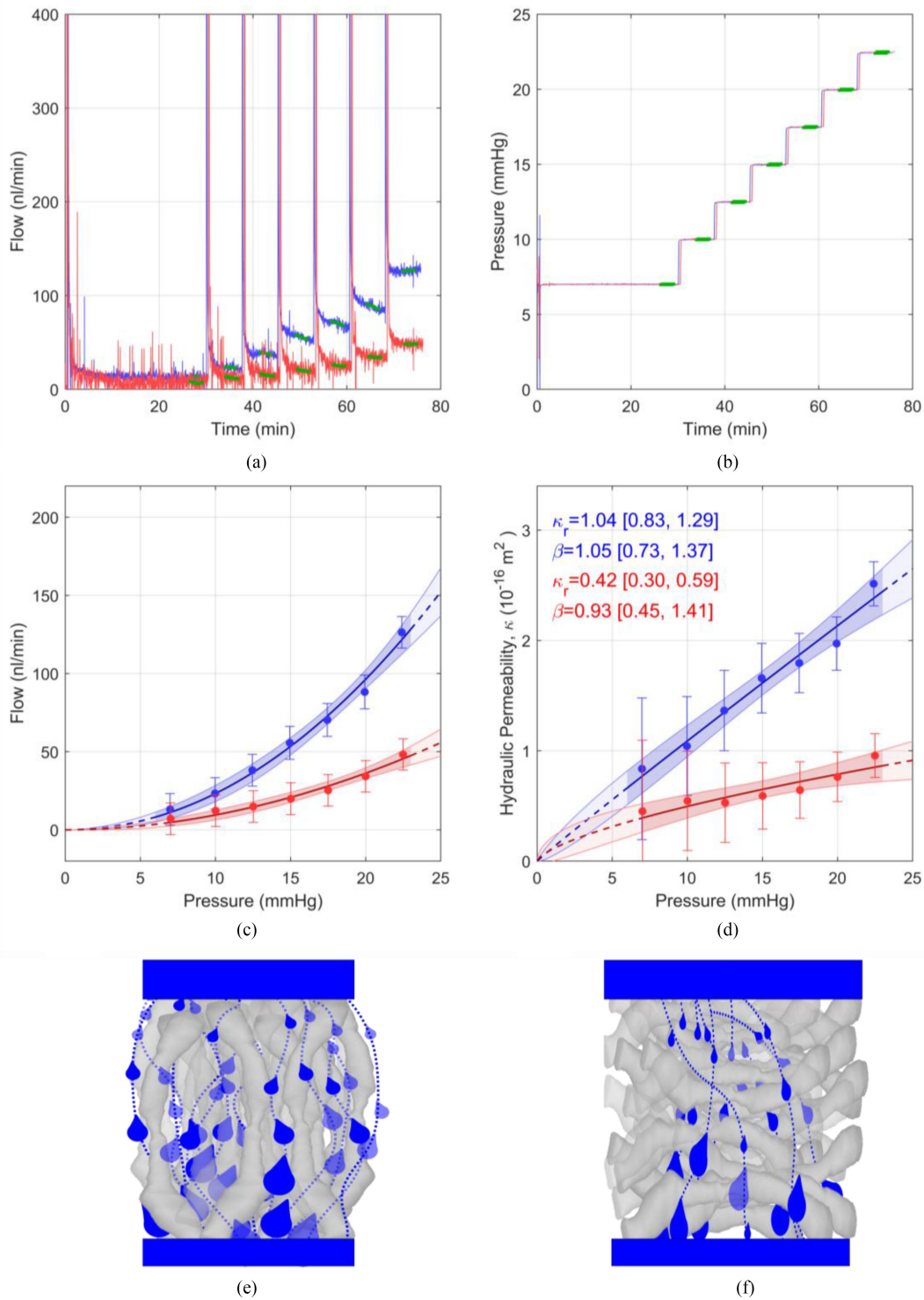


Fig. 2. (a,b) Flow rate and pressure traces of representative $S_{||}$ (blue) and S_{\perp} (red) samples. Green lines show filtered signal. (c) Flow-pressure and (d) hydraulic permeability pressure relationships. Error bars show two standard deviations and shaded regions indicate 95% confidence bounds. The κ_r and β values are the geometric mean with 95% confidence interval at all pressure steps. (e,f) schematic representation showing the flow direction relative to axons orientation for $S_{||}$ and S_{\perp} respectively.

when using different methods to study fluid flow in biological tissue, for example by using fractional order derivatives [55].

The results reported in Fig. 3 and in the additional Supplementary Information clearly demonstrate the difference in

hydraulic permeability between $S_{||}$ and S_{\perp} and thus the dependence of this parameter, and in turn of CED procedures, on the directionality of axons in WM. This strongly encourages to consider the anisotropy of WM tissue when modelling the

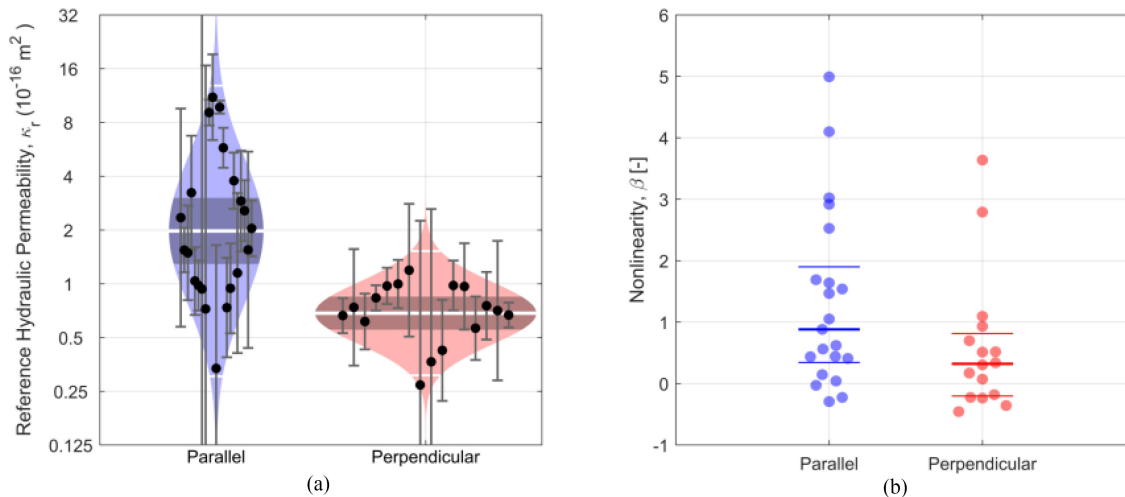


Fig. 3. Hydraulic permeability of S_{\parallel} and S_{\perp} samples and their pressure dependence. (a) Cello plot representing each κ_r value by a dot with the error bars showing 95% confidence intervals, best estimate of the distribution by shaded regions, geometric mean by the central horizontal white line, two-sigma within which 95% data are expected to lie by horizontal out thin white lines and 95% confidence intervals on the mean value by dark central bands, (b) the nonlinearity, β , for S_{\parallel} and S_{\perp} samples; dots represent each data point, central dark line represents the median and out two lines represent the interquartile range (IQR = Q3 - Q1).

localised pressure-flow behaviour in infusion phenomenon and when assessing interstitial transport in brain tissue due to physiological conditions or CED procedures.

B. Pressure Dependence of Hydraulic Permeability

Our data also revealed a pressure-dependence of the hydraulic permeability. Fig. 3(b) shows the non-linearity parameter, β , for both S_{\parallel} and S_{\perp} samples. The Shapiro-Wilk test rejected both normality ($p < 0.03$) and log-normality ($p < 10^{-5}$) for β , hence a non-parametric analysis is utilised. For S_{\parallel} samples, the β was 0.88 (0.34, 1.90) (median (25th percentile, 75th percentile)), which is significantly different from zero ($p = 0.0002$, two-sided Wilcoxon rank sum test), implying that hydraulic permeability increases with increasing pressure. S_{\perp} samples, yielded $\beta = 0.32$ (-0.20, 0.81), which is borderline different from zero, ($p = 0.04$). The median β was therefore 64% lower for S_{\perp} than S_{\parallel} , although this outcome was borderline statistically significant ($p = 0.07$).

The non-linearity in the observed pressure-flow relationships could be caused by several sources, including strain-dependence of hydraulic permeability due to the local tissue response to deformation, but also other material (both solid response to pressure gradients and complex fluid flow behaviour) and geometrical non-linearities, which include the boundary conditions at the infusion site, the cavity formed at the tip of the catheter. Based on macroscale experiments, both, the stiffening behaviour under tension [37] and the softening behaviour [56] in brain tissue due to geometrical non-linearities have been reported in the literature. Several poroelastic or biphasic models of brain tissue have been developed to explain such experimental results. Considering a simplified spherical geometry, Smith *et al.* [57] modelled the enlargement of the infusion sphere relative to its initial radius with increase in applied pressure, which results in geometrical non-linearity. Considering the biomaterial as a

poroelastic medium, McGuire *et al.* [20] performed numerical simulations and showed that strain dependent permeability is anisotropically affected by infusion-induced tissue deformation. It should be noted that the models presented in these studies represent the brain tissue as homogeneous and isotropic and were developed to explain previously reported experimental results based on compression of large samples rather than infusion. They only provide the large-scale bulk response of the tissue and cannot be used to study the effect of microstructurally-induced anisotropy.

It should be noted that in the approach used to calculate of hydraulic permeability the potential effects of localised expansion of WM is not explicitly considered. This is because, although our infused volume is inherently small, it is difficult to quantify the extent by which WM tissue is affected by localised infusion in the present experimental arrangement. The extent to which tissue can expand due to infusion is largely dependent on the treatment and volume of injected infusate [58], [59], cytoarchitectural regions, such as WM or grey matter which promote convective and diffusion flow respectively [49], and pre-existing conditions *e.g.* edema [60]. In WM, convective flow is anisotropic [8] and the preferential distribution of infusate along parallel WM tracts in corona radiata has been used to rapidly fill the cerebral hemisphere [61]. This suggests that if the infusate flow rate is large enough to cause expansion, WM would expand anisotropically, with WM tracts spreading apart but not elongating [26]. This, while implying that hydraulic permeability would be affected by such processes, further highlights the major role of geometrical features in WM, *i.e.* directionality of axons, during infusion. While acknowledging the possible contribution of tissue expansion to hydraulic permeability, considering the small flow rates (in range of nl/min) adopted in the present studies, we believe that this contribution, if existing, is minor. Additionally, in our ex-vivo measurements on dead tissue, in contrast to in-situ measurements reported in the literature [59], interstitial fluid

flow, which usually goes along WM tracts and contribute to intracranial pressure [50] is not present. This further supports our claim that the main difference in hydraulic permeability in S_{\parallel} and S_{\perp} samples is to be attributed to the microscopic geometrical features of the tissue.

It must be noted that another potential source of non-linearity could be the existence of flow along the needle/tissue interface. This form of “leakage”, usually called backflow [7], cannot be completely ruled out in the absence of detailed localized flow measurements; this could be responsible for some of the larger values of β reported in this study. However, the fact that the non-linearity parameter is larger in the specimens characterized by parallel axon fibres (see Fig. 3(b)) shows that the non-linear response depends on the orientation of the fibres whilst leakage would equally affect all samples. This, together with the evidence provided by the studies reported above, gives us reasons to believe that the non-linear pressure dependence reported in our study is likely to be related to the subtleties of infusion-induced microscale deformation of the WM tissue. Further studies, employing direct microscopic measurements of tracked nano- and micro-particles, will be devoted to exploring the main source of the non-linearity of the pressure-flow relationship and to verify the absence of needle side leakage.

C. Effect of Post-Mortem Time on Hydraulic Permeability

The effect of post-mortem time on brain tissue mechanical properties has been reported in literature; however, limited understanding has been developed because of the absence of definitive and uncontroversial results. Several factors including type of measurements, sample properties and physiological conditions potentially contribute to these differences reported in literature. Nicolle *et al.* [62] reported that corona radiata samples stored in physiological solutions at 6 maintained their stiffness when measured at 24h and 48h post-mortem. Using microscale indentation, Budday *et al.* [63] reported less than 5% deviation in stiffness of brain WM when the tissue was kept intact and hydrated between 2h and 5 days post-mortem. However, increase in tissue stiffness with post-mortem time has also been widely reported. Stiffness of samples from thalamus region of brain reported to increase with post-mortem time and specific changes recorded after 6h post-mortem when tested in shear at post-mortem time ranging from 2.5h to 10h however this was also dependent on tissue mechanical history [64]. Weickenmeier *et al.* [65] characterised the in-vivo and in-situ brain stiffness employing magnetic resonance elastography, a non-invasive technique, and reported immediate brain stiffening *e.g.* corpus callosum stiffened up to 58% within three minutes of post-mortem, up to 142% within 45 minutes and up to 274% at 16h. However, their ex-vivo indentation moduli measured on coronal slices of the same brain 16h post-mortem were similar to in-situ moduli 45 minutes post-mortem. Please note here, the tightly regulated mechanical environment to which brain is exposed in-vivo drastically changes when tissue pieces are cut for testing and pre-strain and residual stress are released. Furthermore, the heterogeneous and anisotropic nature of WM,

where small changes in location can change stiffness significantly [66], [67], make interpretation of homogenised information from elastography in context of localised phenomena such as indentation or infusion, ambiguous. It should be noted that most of these indentation studies have looked at relatively large (millimetre sized) samples compared to (micrometre sized) axonal structures, hence reporting homogenised properties and their variation. Additionally, despite comprehensive efforts to reveal effect of post-mortem time on brain tissue stiffening, these studies have not looked at hydraulic permeability in this context. In our study of hydraulic permeability, infusion-based flow is a localised phenomenon and therefore the apparent changes in stiffness from tissue homogenised response should be considered cautiously. Here, we analysed the hydraulic permeability at post-mortem times up to 11h. No statistical correlation between post-mortem time and hydraulic permeability was observed: for S_{\parallel} , $\rho = -0.003$ ($p = 0.99$) and for S_{\perp} , $\rho = -0.09$ ($p = 0.7$) using Spearman’s ranked correlation test.

It should be noted here that whilst the results reported in this study were consistent for experiments performed within 11h post-mortem, the maximum number of samples which passed the quality control measures were not equally distributed within the post-mortem window analysed here, *i.e.* 32 were tested at <6h post-mortem, followed by 10 samples between 6h and 8h and only a few samples between 8h and 11h. This suggests that local microstructural changes in the context of hydraulic permeability become relevant after 6h post-mortem. Experiments performed after 11h post-mortem either failed by showing significant anomalies in the instantaneous response to pressure steps or registered sudden abrupt changes in flow, which can be reconnected to tissue rupture during testing, and none of these experiments passed the quality control measures to be included in the data analysis.

IV. CONCLUSION

The localised hydraulic permeability of brain WM, despite being a key parameter for the development of infusion-based technologies, has so far not been systematically studied experimentally. In this work we investigated for the first time the effect of local microstructural features on hydraulic permeability of cerebral WM in a systematic manner using an infusion based experimental set up. We accounted for the directionality of axons in WM and showed the dependence of hydraulic permeability on the anisotropy in WM tissue. We also investigated whether it is affected by post-mortem time.

Our results demonstrate that the mean value of hydraulic permeability is significantly lower *i.e.* 65% ($p = 0.0002$, mean, [95% CI]), when the flow is perpendicular to the axons in WM than when the flow is parallel to the axons. We also observed a pressure dependent increase in hydraulic permeability, with median nonlinearity parameter β being 64% ($p = 0.07$) lower when axon in WM are perpendicular to the flow direction than when axons are parallel to the flow direction. Although there was no correlation between hydraulic permeability and post-mortem time within 11h, the tissue degradation at later times significantly affected our ability to measure hydraulic permeability after 11h.

Our experimental results provide quantitative values of hydraulic permeability as a function of the direction of the WM fibre bundles from directly measured parameters. While this has been reported theoretically and anisotropy of permeability has been considered to explain some features of CED, no experimental evidence existed so far to demonstrate and quantify such effect. These can be used to enhance the development of technologies such as CED and as a prime source of information to build detailed mechanical models of brain tissue. Additionally, this investigation provides further evidence of the need to include tissue anisotropy as one of the key parameters for the optimization of infusion-based drug delivery techniques.

REFERENCES

- [1] N. A. O. Bush, S. M. Chang, and M. S. Berger, "Current and future strategies for treatment of glioma," *Neurosurg. Rev.*, vol. 40, no. 1, pp. 1–14, 2017.
- [2] E. Alphandéry, "Glioblastoma treatments: An account of recent industrial developments," *Front. Pharmacol.*, vol. 9, pp. 1–31, Sep. 2018.
- [3] B. G. Harder *et al.*, "Developments in blood-brain barrier penetrance and drug repurposing for improved treatment of Glioblastoma," *Front. Oncol.*, vol. 8, pp. 1–10, Oct. 2018.
- [4] U. H. Weidle, J. Niewohner, and G. Tiefenthaler, "The blood-brain barrier challenge for the treatment of brain cancer, secondary brain metastases, and neurological diseases," *Cancer Genomics Proteomics*, vol. 12, no. 4, pp. 167–178, 2015.
- [5] F. Yuan, "Transvascular drug delivery in solid tumors," *Semin. Radiat. Oncol.*, vol. 8, no. 3, pp. 164–175, 1998.
- [6] M. Terzano *et al.*, "An adaptive finite element model for steerable needles," *Biomech. Model. Mechanobiol.*, no. 0123456789, Mar. 2020.
- [7] M. A. Audette, S. P. Bordas, and J. E. Blatt, "Robotically steered needles: A survey of neurosurgical applications and technical innovations," *Robot. Surg. Res. Rev.*, vol. 7, pp. 1–23, Mar. 2020.
- [8] R. R. Lonser *et al.*, "Convection-enhanced delivery to the central nervous system," *J. Neurosurg.*, vol. 122, no. 3, pp. 697–706, Mar. 2015.
- [9] A. M. Mehta, A. M. Sonabend, and J. N. Bruce, "Convection-enhanced delivery," *Neurotherapeutics*, vol. 14, no. 2, pp. 358–371, 2017.
- [10] A. Healy and M. Vogelbaum, "Convection-enhanced drug delivery for gliomas," *Surg. Neurol. Int.*, vol. 6, no. 2, pp. S59–S67, 2015.
- [11] R. Raghavan *et al.*, "Convection-enhanced delivery of therapeutics for brain disease, and its optimization," *Neurosurg. Focus*, vol. 20, no. 4, Apr. 2006, Paper E12.
- [12] X. Chen and M. Sarnintoranont, "Biphasic finite element model of solute transport for direct infusion into nervous tissue," *Ann. Biomed. Eng.*, vol. 35, no. 12, pp. 2145–2158, 2007.
- [13] G. Miranpuri *et al.*, "Convection enhanced delivery: A comparison of infusion characteristics in ex vivo and in vivo non-human primate brain tissue," *Ann. Neurosci.*, vol. 20, no. 3, pp. 108–114, 2013.
- [14] R. Raghavan and R. M. Odland, "Theory of porous catheters and their applications in intraparenchymal infusions," *Biomed. Phys. Eng. Express*, vol. 3, no. 2, Feb. 2017, Art. no. 025008.
- [15] L. Ray, J. J. Iliff, and J. J. Heys, "Analysis of convective and diffusive transport in the brain interstitium," *Fluids Barriers CNS*, vol. 16, no. 1, pp. 1–18, 2019.
- [16] E. Syková and C. Nicholson, "Diffusion in brain extracellular space," *Physiol. Rev.*, vol. 88, no. 4, pp. 1277–1340, 2008.
- [17] H. Mestre *et al.*, "Cerebrospinal fluid influx drives acute ischemic tissue swelling," *Science (80-.)*, vol. 367, no. 6483, Mar. 2020, Art. no. eaax7171.
- [18] L. Vargová and E. Syková, "Extracellular space diffusion and extrasynaptic transmission," *Physiol. Res.*, vol. 57, no. SUPPL. 3, pp. S89–S99, 2008.
- [19] L. F. Agnati, B. Bjelke, and K. Fuxe, "Volume transmission in the brain," *Am. Sci.*, vol. 80, no. 4, pp. 362–373, 1992.
- [20] S. McGuire, D. Zaharoff, and F. Yuan, "Nonlinear dependence of hydraulic conductivity on tissue deformation during intratumoral infusion," *Ann. Biomed. Eng.*, vol. 34, no. 7, pp. 1173–1181, Jul. 2006.
- [21] A. K. Datta, "Hydraulic permeability of food tissues," *Int. J. Food Prop.*, vol. 9, no. 4, pp. 767–780, 2006.
- [22] M. Vidotto *et al.*, "A computational fluid dynamics approach to determine white matter permeability," *Biomech. Model. Mechanobiol.*, vol. 18, no. 4, pp. 1111–1122, 2019.
- [23] A. C. R. Tavner *et al.*, "On the appropriateness of modelling brain parenchyma as a biphasic continuum," *J. Mech. Behav. Biomed. Mater.*, vol. 61, pp. 511–518, 2016.
- [24] W. Ehlers and A. Wagner, "Multi-component modelling of human brain tissue: A contribution to the constitutive and computational description of deformation, flow and diffusion processes with application to the invasive drug-delivery problem," *Comput. Methods Biomech. Biomed. Eng.*, vol. 18, no. 8, pp. 861–879, 2015.
- [25] K. H. Støverud *et al.*, "Modeling concentration distribution and deformation during convection-enhanced drug delivery into brain tissue," *Transp. Porous Media*, vol. 92, no. 1, pp. 119–143, 2012.
- [26] R. Raghavan and M. Brady, "Predictive models for pressure-driven fluid infusions into brain parenchyma," *Phys. Med. Biol.*, vol. 56, no. 19, pp. 6179–6204, 2011.
- [27] A. A. Linninger *et al.*, "Computational methods for predicting drug transport in anisotropic and heterogeneous brain tissue," *J. Biomech.*, vol. 41, no. 10, pp. 2176–2187, 2008.
- [28] V. Vetri *et al.*, "Advanced microscopy analysis of the micro-nanoscale architecture of human menisci," *Sci. Rep.*, vol. 9, no. 1, p. 18732, Dec. 2019.
- [29] O. Barrera, E. Bologna, M. Zingales, and G. Alotta, "Experimental characterization of the human meniscal tissue," in *Proc. IEEE 4th Int. Forum Res. Technol. Soc. Industry*, 2018, pp. 1–5.
- [30] Y. Boucher *et al.*, "Intratumoral infusion of fluid: Estimation of hydraulic conductivity and implications for the delivery of therapeutic agents," *Br. J. Cancer*, vol. 78, no. 11, pp. 1442–1448, 1998.
- [31] X. Y. Zhang, J. Luck, M. W. Dewhirst, and F. Yuan, "Interstitial hydraulic conductivity in a fibrosarcoma," *Am. J. Physiol. - Hear. Circ. Physiol.*, vol. 279, no. 6 48-6, pp. 2726–2734, 2000.
- [32] M. Milosevic *et al.*, "Interstitial permeability and elasticity in human cervix cancer," *Microvasc. Res.*, vol. 75, no. 3, pp. 381–390, 2008.
- [33] P. Heneghan and P. E. Riches, "Determination of the strain-dependent hydraulic permeability of the compressed bovine nucleus pulposus," *J. Biomech.*, vol. 41, no. 4, pp. 903–906, 2008.
- [34] B. Reynaud and T. M. Quinn, "Anisotropic hydraulic permeability in compressed articular cartilage," *J. Biomech.*, vol. 39, no. 1, pp. 131–137, 2006.
- [35] F. LE Vunjak-Novakovic G *et al.*, "Bioreactor cultivation conditions modulate the composition and mechanical properties of tissue-engineered cartilage," *J. Orthop. Res.*, vol. 17, no. 1, pp. 130–138, 1999.
- [36] W. Y. Gu and H. Yao, "Effects of hydration and fixed charge density on fluid transport in charged hydrated soft tissues," *Ann. Biomed. Eng.*, vol. 31, no. 10, pp. 1162–1170, 2003.
- [37] G. Franceschini *et al.*, "Brain tissue deforms similarly to filled elastomers and follows consolidation theory," *J. Mech. Phys. Solids*, vol. 54, no. 12, pp. 2592–2620, 2006.
- [38] K. B. Walhovd, H. Johansen-Berg, and R. T. Káradóttir, "Unraveling the secrets of white matter - Bridging the gap between cellular, animal and human imaging studies," *Neuroscience*, vol. 276, pp. 2–13, 2014.
- [39] V. Pieri *et al.*, "In vivo diffusion tensor magnetic resonance tractography of the sheep brain: An atlas of the ovine white matter fiber bundles," *Front. Vet. Sci.*, vol. 6, no. October, pp. 1–15, 2019.
- [40] W. Zhan, F. Rodriguez y Baena, and D. Dini, "Effect of tissue permeability and drug diffusion anisotropy on convection-enhanced delivery," *Drug Del.*, vol. 26, no. 1, pp. 773–781, 2019.
- [41] J. M. Sherwood *et al.*, "Measurement of outflow facility using iPerfusion," *PLoS One*, vol. 11, no. 3, pp. 1–29, 2016.
- [42] L. T. Dunn, "Raised intracranial pressure," *J. Neurol. Neurosurg. Psychiatry*, vol. 73, no. suppl 1, pp. i23–i27, Sep. 2002.
- [43] C. R. Ethier, "Flow through mixed fibrous porous materials," *AICHE J.*, vol. 37, no. 8, pp. 1227–1236, 1991.
- [44] E. Syková and C. Nicholson, "Diffusion in brain extracellular space," *Physiol. Rev.*, vol. 88, no. 4, pp. 1277–1340, Oct. 2008.
- [45] D. C. Alexander *et al.*, "Imaging brain microstructure with diffusion MRI: Practicality and applications," *NMR Biomed.*, no. Nov. 2016, pp. 1–26, 2017.
- [46] H. Ouyang, E. Nauman, and R. Shi, "Contribution of cytoskeletal elements to the axonal mechanical properties," *J. Biol. Eng.*, vol. 7, no. 1, pp. 1–8, 2013.
- [47] R. G. Wells, "The role of matrix stiffness in regulating cell behavior," *Hepatology*, vol. 47, no. 4, pp. 1394–1400, 2008.
- [48] N. J. Abbott, "Evidence for bulk flow of brain interstitial fluid: Significance for physiology and pathology," *Neurochem. Int.*, vol. 45, no. 4, pp. 545–552, 2004.

- [49] C. P. Geer and S. A. Grossman, "Interstitial fluid flow along white matter tracts: A potentially important mechanism for the dissemination of primary brain tumors," *J. Neurooncol.*, vol. 32, no. 3, pp. 193–201, 1997.
- [50] C. A. Stine and J. M. Munson, "Convection-enhanced delivery: Connection to and impact of interstitial fluid flow," *Front. Oncol.*, vol. 9, pp. 1–15, Oct. 2019.
- [51] H. Rappel and L. A. A. Beex, "Estimating fibres' material parameter distributions from limited data with the help of Bayesian inference," *Eur. J. Mech. - A/Solids*, vol. 75, pp. 169–196, May 2019.
- [52] H. Rappel, L. A. A. Beex, and S. P. A. Bordas, "Bayesian inference to identify parameters in viscoelasticity," *Mech. Time-Dependent Mater.*, vol. 22, no. 2, pp. 221–258, May 2018.
- [53] H. Rappel *et al.*, "A tutorial on Bayesian inference to identify material parameters in solid mechanics," *Arch. Comput. Methods Eng.*, vol. 27, no. 2, pp. 361–385, Apr. 2020.
- [54] M. Mohamedou *et al.*, "Bayesian identification of mean-field homogenization model parameters and uncertain matrix behavior in non-aligned short fiber composites," *Compos. Struct.*, vol. 220, pp. 64–80, Jul. 2019.
- [55] R. L. Magin *et al.*, "Characterization of anomalous diffusion in porous biological tissues using fractional order derivatives and entropy," *Microporous Mesoporous Mater.*, vol. 178, pp. 39–43, Sep. 2013.
- [56] K. Miller and K. Chinzei, "Mechanical properties of brain tissue in tension," *J. Biomech.*, vol. 35, no. 4, pp. 483–490, 2002.
- [57] J. H. Smith and J. J. García, "A nonlinear biphasic model of flow-controlled infusion in brain: Fluid transport and tissue deformation analyses," *J. Biomech.*, vol. 42, no. 13, pp. 2017–2025, 2009.
- [58] M. L. Brady *et al.*, "Large-volume infusions into the brain: A comparative study of catheter designs," *Stereotact. Funct. Neurosurg.*, vol. 96, no. 3, pp. 135–141, 2018.
- [59] M. Brady *et al.*, "Quantifying fluid infusions and tissue expansion in brain," *IEEE Trans. Biomed. Eng.*, vol. 58, no. 8, pp. 2228–2237, Aug. 2011.
- [60] J. H. Sampson *et al.*, "Induction of hyperintense signal on T2-weighted MR images correlates with infusion distribution from intracerebral convection-enhanced delivery of a tumor-targeted cytotoxin," *Am. J. Roentgenol.*, vol. 188, no. 3, pp. 703–709, Mar. 2007.
- [61] R. R. Lonser *et al.*, "Convection perfusion of glucocerebrosidase for neuropathic Gaucher's disease," *Ann. Neurol.*, vol. 57, no. 4, pp. 542–548, Apr. 2005.
- [62] S. Nicolle *et al.*, "Shear linear behavior of brain tissue over a large frequency range," *Biorheology*, vol. 42, no. 3, pp. 209–223, 2005.
- [63] S. Budday *et al.*, "Mechanical properties of gray and white matter brain tissue by indentation," *J. Mech. Behav. Biomed. Mater.*, vol. 46, pp. 318–330, Jun. 2015.
- [64] A. Garo *et al.*, "Towards a reliable characterisation of the mechanical behaviour of brain tissue: The effects of post-mortem time and sample preparation," *Biorheology*, vol. 44, no. 1, pp. 51–58, 2007.
- [65] J. Weickenmeier *et al.*, "Brain stiffens post mortem," *J. Mech. Behav. Biomed. Mater.*, vol. 84, no. April, pp. 88–98, Aug. 2018.
- [66] J. Weickenmeier *et al.*, "Brain stiffness increases with myelin content," *Acta Biomater.*, vol. 42, pp. 265–272, Sep. 2016.
- [67] S. Budday *et al.*, "Mechanical characterization of human brain tissue," *Acta Biomater.*, vol. 48, pp. 319–340, Jan. 2017.